Pervasive Crustal Volcanic Mush in the Highly Stretched Sunda Plate Margin of Northern Sumatra

Citation for published version:
Feng, M, Wei, S, Chen, L, Muksin, U, Lythgoe, K, Wang, T & Wu, Z 2023, 'Pervasive Crustal Volcanic Mush in the Highly Stretched Sunda Plate Margin of Northern Sumatra', *Geophysical Research Letters*, vol. 50, no. 21, e2023GL104391. https://doi.org/10.1029/2023GL104391

Digital Object Identifier (DOI):
10.1029/2023GL104391

Link:
Link to publication record in Edinburgh Research Explorer

Document Version:
Publisher's PDF, also known as Version of record

Published In:
Geophysical Research Letters

ADVANCING EARTH AND SPACE SCIENCES

Geophysical Research Letters

RESEARCH LETTER
10.1029/2023GL104391

Pervasive Crustal Volcanic Mush in the Highly Stretched Sunda Plate Margin of Northern Sumatra

Mingye Feng[1,2,3,4], Shengji Wei[3,4], Ling Chen[1,2], Umar Muksin[5], Karen Lythgoe[3,4], Tuo Wang[1], and Zimu Wu[6]

[1]State Key Laboratory of Lithospheric Evolution, Institute of Geology and Geophysics, Chinese Academy of Sciences, Beijing, China, [2]College of Earth and Planetary Sciences, University of Chinese Academy of Sciences, Beijing, China, [3]Earth Observatory of Singapore, Nanyang Technological University, Singapore, Singapore, [4]Asian School of the Environment, Nanyang Technological University, Singapore, Singapore, [5]Tsunami and Disaster Mitigation Research Center (TDMRC), Universitas Syiah Kuala, Banda Aceh, Indonesia, [6]Department of Earth and Space Sciences, Southern University of Science and Technology, Shenzhen, China

Key Points:

- A new receiver function method is developed to constrain crustal thickness and melt fraction
- Applications to dense nodal array data in northwestern Sumatra show a thin (~22 km) crust and high crustal melt fraction (up to 19%)
- The new constraints partly explain abnormal volcanic migration and crustal stretching

Supporting Information:

Supporting Information may be found in the online version of this article.

Correspondence to:

S. Wei and L. Chen,
shjwei@ntu.edu.sg;
lchen@mail.iggcas.ac.cn

Citation:

Feng, M., Wei, S., Chen, L., Muksin, U., Lythgoe, K., Wang, T., & Wu, Z. (2023). Pervasive crustal volcanic mush in the highly stretched Sunda plate margin of northern Sumatra. *Geophysical Research Letters*, *50*, e2023GL104391. https://doi.org/10.1029/2023GL104391

Received 4 MAY 2023
Accepted 23 OCT 2023

Abstract

Arc volcanism, crustal deformation, and their interplay are poorly understood in northwestern Sumatra. Traditional receiver function H-κ stacking studies constrain the variations in crustal thickness and V_p/V_s ratio in volcanic zones but rarely estimate the melt fractions. Here, we propose a H-Φ stacking method, a variant of the H-κ stacking method, and apply it to the dense nodal array data from Aceh, northern Sumatra, to estimate crustal thickness, V_p/V_s ratio, and melt fraction. Most results show considerably high V_p/V_s ratios (~1.98) and melt fractions (up to 19%), indicating pervasive crustal magmatic mush. The northwestern edge of the Aceh crust is much thinner (~22 km) than extended crust globally, reflecting a highly stretched crust due to tectonic processes governing the opening of the Andaman Sea. This thin crust and high melt fractions explain the Bouguer gravity anomaly, and partly explain the northward migration of Quaternary volcanics.

Plain Language Summary

Crustal thickness and melt fraction are important indicators of crustal magmatism and deformation. Situated between the Sumatran and Andaman subduction zones, Aceh, in northwestern Sumatra, is distinguished by strong crustal deformation, resulting in active crustal seismicity, and Quaternary volcanics that have migrated northward over time. However, the abnormal arc volcanism, crustal deformation, and their interplay, remain unclear because of poor understanding of the crustal structure. To fill this knowledge gap, we deployed 155 nodal seismic stations in Aceh for 18 months. In this work, we develop a new receiver function method that takes advantage of converted seismic energy from the base of the crust to constrain the crustal thickness and melt fraction beneath the stations in Aceh. We find that: (a) the average crustal melt fraction is as high as 19%, indicating a considerable volume of partially molten rock in the crust and (b) the crust in northern Aceh is as thin as ~22 km, suggesting high stretching of the crust associated with the opening of the Andaman Sea. The stretched crust with a high melt fraction partly explains the northward migration of Quaternary volcanics and active seismicity/crustal deformation, but the migration mechanism of other volcanics requires further investigation.

1. Introduction

Fundamental crustal structure parameters (e.g., V_p/V_s ratio and crustal thickness) are critical to understanding the deformation and volcanism in the overriding plate of a subduction zone. Improved knowledge of crustal structure is particularly needed for northwestern Sumatra (i.e., Aceh), where volcanism has abnormally migrated from the forearc to backarc, for example, the Seulawah Agam, Peuet Sague, and Geureudong volcanoes (Figures 1b and 1c; Lai et al., 2021). However, only sparse seismic observations were previously available, limiting our understanding of the arc volcanism. Important factors, such as the magma budget, distribution, and spatial correlation with the crustal structure and deformation are poorly known (Annen et al., 2006; Cashman et al., 2017).

Aceh is located at the continental margin between the Sunda Arc and the Andaman Sea, accommodating forces of seafloor spreading and far-field extrusion from the north (Figure 1a; X. Wang et al., 2022). The eastern edge of the Andaman Sea shows remarkable correspondence to the big bend of the Sunda trench (Figure 1a). The change in trench curvature also marks the rupture boundary between the 2004 Mw9.2 Sumatra-Andaman and the 2005 Mw8.7 Nias megathrust earthquakes (Chlieh et al., 2007; Hsu et al., 2006) (Figure 1b). Such dramatic structure variations both to the north and south of Aceh cause a high level of seismicity in the northwestern end

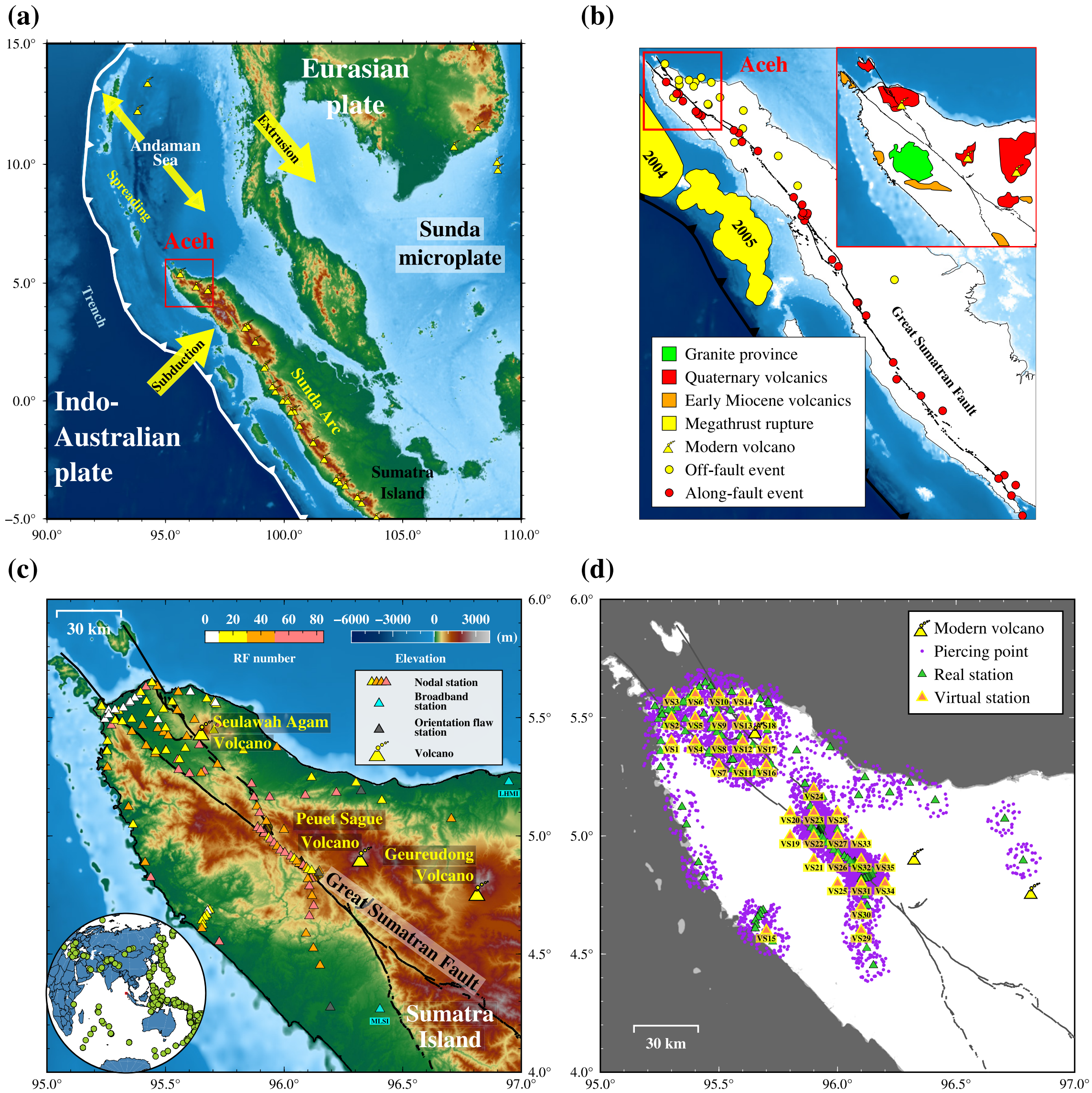

Figure 1. (a and b) Tectonic setting of Aceh, (c and d) distribution of the nodal seismic array. Red and yellow dots in (b) show historical M5.5+ earthquakes along and off the Great Sumatran Fault, respectively (Muzli et al., 2018). Yellow zones in (b) show the 2004 Mw9.2 and 2005 Mw8.7 great earthquake ruptures. Locations of the granite province and volcanics are retrieved from Barber (2000) and Lai et al. (2021), respectively. Gray triangles in (c) show the nodal stations with misorientations of >50°, and the green dots show teleseismic events used. Purple circles in (d) show Ps-wave piercing points at 30 km depth.

of Sumatra (Muksin et al., 2019; Muzli et al., 2018). Sizable off-Sumatran fault crustal earthquakes occur much more frequently in Aceh than in other Sumatran regions, suggesting more distributed deformation in the crust (Figure 1b; Muzli et al., 2018). While both volcanism and crustal deformation highlight the active tectonics of Aceh, the paucity of regional seismic observations has hindered our ability to constrain the crustal structure and thus better understand the tectonics. To fill the observational gap, a dense array of short-period seismic nodes was deployed in Aceh for ~1.5 years, covering the Seulawah Agam Volcano and part of the Great Sumatran Fault (GSF) and its bifurcations (Figure 1c). The array recorded numerous teleseismic earthquakes, providing a valuable data set to better constrain the regional crustal structure.

Typically, crustal structural parameters such as crustal thickness and V_p/V_s ratio are estimated by H-κ stacking of teleseismic receiver functions (RFs) (e.g., Zhu & Kanamori, 2000), which usually reveal high V_p/V_s ratios in volcanic areas (e.g., Eagar et al., 2011; Janiszewski et al., 2013; T. Wang et al., 2021). The high V_p/V_s ratios can indicate the degree of crustal magma mush. Reed et al. (2014) converts V_p/V_s ratio to melt fraction by a theoretical relationship (Watanabe, 1993), which was designed for granitic and rhyolitic melts and thus is not generalizable to other volcanic settings. Hammond (2014) extends H-κ stacking to constrain melt-induced crustal anisotropy, providing estimates for melt fraction by considering the aspect ratio of the melt. However, the study finds a strong trade-off between melt fraction and melt geometry (aspect ratio).

To resolve these limitations, here we propose both explicit and implicit approaches to estimate the crustal melt fraction, based on critical porosity and Gassmann's equations (Gassmann, 1951; Nur et al., 1998). Critical porosity is equivalent to aspect ratio in parameterizing velocity by melt fraction, with the advantage that it can be determined by geological information to better resolve the trade-off between melt fraction and melt geometry (Paulatto et al., 2022). The explicit method directly converts V_p/V_s ratio into melt fraction, while the implicit method incorporates Gassmann's equations into H-κ stacking method to constrain crustal thickness, melt fraction, V_p, and V_p/V_s ratio simultaneously. We name the implicit method as H-Φ stacking method and apply it to the nodal seismic array data in Aceh. Based on the crustal thickness result, the crustal stretching factor is also estimated. We then analyze the interaction between crustal stretching and magmatic mush distribution. In the following sections, we first introduce the data and the methods, then show our results, followed by interpretation regarding the spatial distribution of magmas, regional tectonic, and volcanic processes.

2. RF Data

The short-period array comprises 155 nodes, deployed from January 2020 to July 2021 (Figure 1c) and principally distributed along roads and flat areas. The deployment team overcame difficulties imposed by the tropical environment and the COVID19 pandemic, managing to recharge and re-deploy all nodes every ∼35 days. This is a unique way of deploying nodal arrays for long-term acquisition over many cycles of node's battery life (Lythgoe et al., 2022). Beside the short-period array, we also include two permanent broadband stations (MLSI and LHMI) in Aceh for RF analysis. Waveform data are collected for teleseismic events (28–92° epicentral distance) that occurred during the deployment period and have magnitudes ≥5.5 (Figure 1c). Before RF analysis, we detect the sensor misorientation (Niu & Li, 2011; X. Wang et al., 2016) and exclude the nodal stations with >30° misorientations (Figures S1 and S2 in Supporting Information S1). For broadband station MLSI, we detect a 202 ± 6.7° misorientation and correct it (Figures S3 and S4 in Supporting Information S1).

We calculate RFs from the teleseismic waveforms with a time domain iterative deconvolution method (Kikuchi & Kanamori, 1992; Ligorría & Ammon, 1999). We then select high-quality RFs rigorously by both visual inspection and automatic selection. In total, we obtain >5,700 high-quality RFs (see more details on data pre-processing in Text S1 of Supporting Information S1). We find eight nodal stations that show clear reverberation phases, suggesting the presence of unconsolidated sediments (Langston, 2011; Y. Yu et al., 2015; Zelt & Ellis, 1999). The reverberations are suppressed by a frequency domain filtering algorithm (Y. Yu et al., 2015) (Figures S5 and S6 in Supporting Information S1).

3. Methods

3.1. Virtual Station H-κ Stacking With Multiple Parameters

Our nodal array observations have a high level of noise, likely due to the poor deployment condition. Fortunately, the dense array allows for spatial stacking to increase the signal-to-noise ratio (SNR) (Lythgoe et al., 2020; Ward et al., 2018). Here we apply a spatial stacking technique, called "Virtual Station Stacking," to group RF traces. For a single station, the spatial resolution of traditional H-κ stacking depends on the distribution of Ps conversion points at the Moho. Assuming a crustal V_s of 3.5 km/s and a crustal thickness of 30 km, the horizontal resolution of H-κ stacking is ∼20 km. To cover piercing points with similar resolution, we group RFs within each 10-km-radius cylinder, inside which the RF number is required to be ≥100. In total, 35 virtual stations are established (Figure 1d). The Moho piercing points are calculated based on a regional forearc velocity model (Collings et al., 2012) (Figure S7b in Supporting Information S1). Figure 2a shows that the virtual station stacking significantly enhances the SNR.

We then apply H-κ stacking to the virtual station RFs to estimate the best crustal thickness and V_p/V_s ratio fitting the traveltimes of Ps, PpPs, and PsPs + PpSs phases from the Moho (Zhu & Kanamori, 2000). We assume that reliable crustal thickness range, V_p/V_s ratio range, and crustal V_p are 20–50 km, 1.5–2.3, 6.1 km/s, respectively, according to previous studies (e.g., Bora et al., 2016; Laske et al., 2012; Macpherson et al., 2012; Pratama et al., 2020). H-κ stacking is established hypothesizing a single-layer and isotropic crust, which may lead to relatively large uncertainties in areas

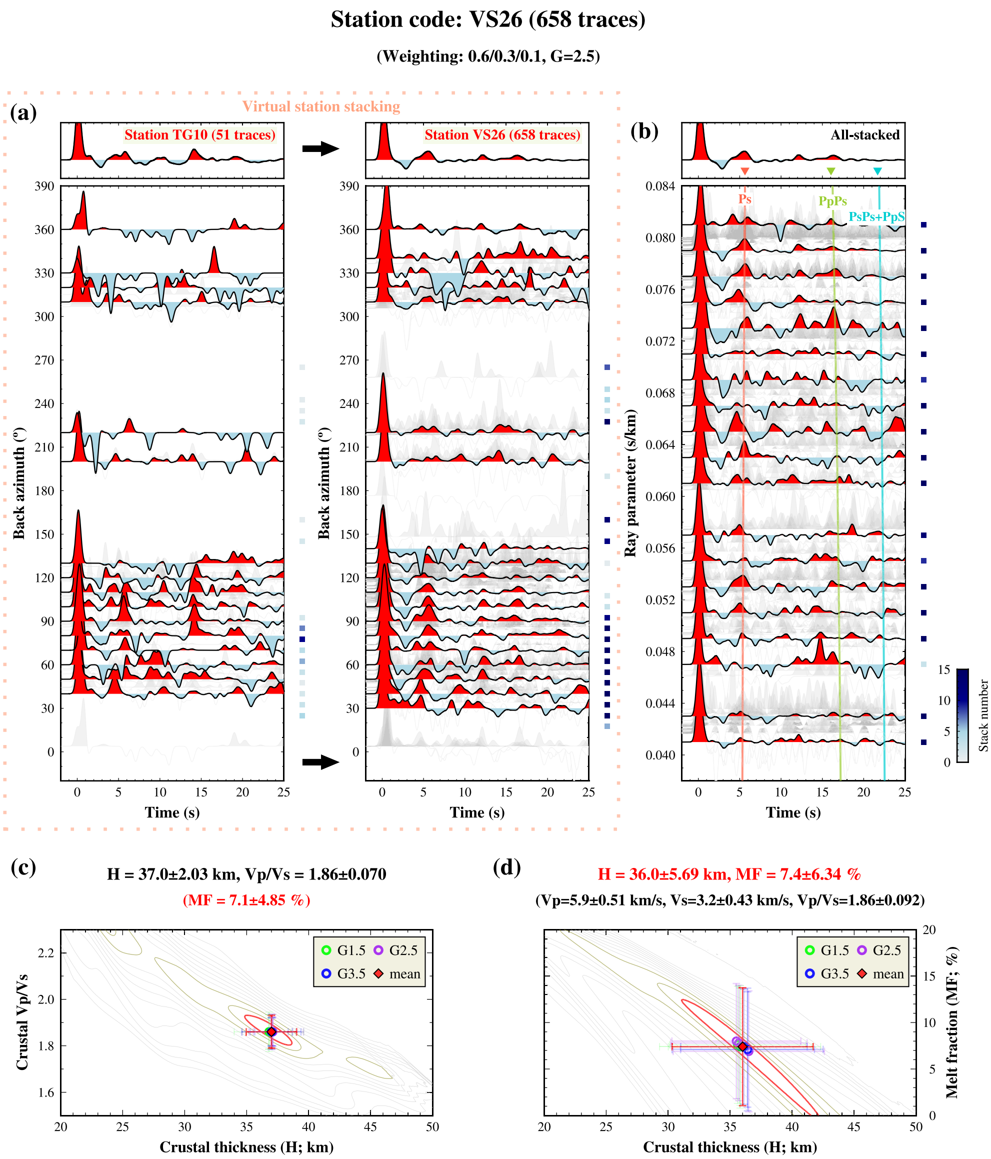

Figure 2. (a) Virtual station stacking and (b–d) results of multiple-parameter H-κ stacking and H-Φ stacking at VS26. Panel (a) shows the comparison of receiver functions (RFs) at real station TG10 and virtual station VS26, which are located very closely (Figure S7a in Supporting Information S1). Gray and color-filled waveforms show individual and stacked RFs, respectively. The number of RFs stacked in back azimuthal or ray parameter bins is shown by the squares. The theoretical arrival times of target phases in H-κ and H-Φ stacking are marked by the lines and the triangles, respectively. Panels (c and d) are the H-κ and H-Φ stacking results, respectively. "MF" means melt fraction. The circles show estimates from various Gaussian filtering (G) and weighting parameters. The estimates are grouped by G and shown in green, purple, and blue. The 95% energy contour is marked in red, and the 80% and 90% contours are marked in brown.

with complex tectonic settings, manifesting as non-unique H-κ estimates (Figure S8 in Supporting Information S1; Ogden et al., 2019). To suppress this non-uniqueness, we apply different Gaussian filtering and weighting parameters (Figures 2b and 2c; Feng et al., 2021; Ogden et al., 2019). The final estimate is defined as the average of the results derived from different parameters. The final uncertainty is the average uncertainty of individual results estimated by the 95% contour of the stacked energy (Figure 2c). See more details in Text S2 of Supporting Information S1.

3.2. Explicit and Implicit Approaches for Melt Fraction Estimation

We derive both the explicit and implicit expressions of melt fraction based on Gassmann's equations (Gassmann, 1951) and the assumption of critical porosity (Nur et al., 1998). Gassmann's equations describe the relationship between melt fraction and velocity under a low-frequency assumption that poral fluids fully fill the pore space (Chu et al., 2010). Critical porosity defines the transition porosity where a frame-supported medium turns to be fluid-supported (Van der Molen & Paterson, 1979). Melt fraction (Φ) can be expressed as a function of V_p/V_s ratio (κ):

$$\Phi = \Phi_0 - \frac{A}{B}$$

$$A = K_0 \Phi_0 K_m$$

$$B = \Phi_0 (K_0 - K_m)(C\mu_0 - K_0) + K_m C \mu_0$$

$$C = \kappa^2 - \frac{4}{3}$$

where K_0, μ_0, K_m, Φ_0, κ are the bulk and shear moduli of the country rock, the bulk modulus of melt, the critical porosity, and the V_p/V_s ratio, respectively. The sensitivity kernel between Φ and κ is defined by the derivative of melt fraction with respect to κ:

$$\partial \Phi = \frac{2AD}{B^2} \kappa \partial \kappa$$

$$D = \mu_0 \Phi_0 (K_0 - K_m) + K_m \mu_0$$

where K_0, μ_0 are converted from the seismic wave speeds and density of the country rock (Chu et al., 2010). Based on a regional velocity model and the exposure of dacite-andesite rocks in northern Sumatra, we assume a V_p value of 6.5 km/s and V_p/V_s ratio of 1.78 for the country rock (Ji et al., 2009; Kennett et al., 1995; Laske et al., 2012; Rock et al., 1982; Zaini et al., 2021). K_m and ϕ_0 are assigned to be 16.1 GPa (e.g., for andesitic melt; Bass, 1995) and 0.30 (e.g., for dacite volcanos; X. Yu & Lee, 2016), respectively. Based on these equations, when country rock parameters and melt parameters are fixed, Φ only depends on κ. Here κ could be estimated by H-κ stacking or other approaches.

Based on the above explicit relationship between Φ and κ, we further expand the traditional H-κ stacking method to a H-Φ stacking method, which is an implicit approach to estimate the average crustal melt fraction. Note that in H-κ stacking a constant crustal V_p is assumed, which is inappropriate since the average crustal V_p decreases as the melt fraction increases (Figure S9 in Supporting Information S1). In our proposed H-Φ stacking method, the crustal V_p is estimated based on the melt fraction, therefore the V_p is no longer constant. This is an improvement on the traditional H-κ method, resulting in a more accurate crustal thickness estimate.

We implement H-Φ stacking of RFs through the following steps. First, assuming the density, shear and bulk moduli of the country rock, density and bulk modulus of the melt, and critical porosity, Gassmann's equations are applied for a range of melt fraction to calculate the corresponding V_p and V_s. Second, based on these velocities, the theoretical arrival times of the three target phases are calculated for a range of crustal thickness (H). These phases are then stacked with assigned weights (similar to that in H-κ stacking). The largest stacking energy provides the optimal estimation for crustal thickness and melt fraction. In this process, V_p, V_s, and V_p/V_s are estimated as byproducts (Figure 2d and Figure S10 in Supporting Information S1).

We evaluate the robustness of H-Φ stacking through a series of synthetic tests. We use V_p = 6.5 km/s, V_p/V_s = 1.78, density = 2.75 g/cm^3 for the country rock, density = 2.45 g/cm^3, bulk modulus = 16.1 GPa for the melt, and critical porosity of 0.3 (N1 model in Table S1 of Supporting Information S1) as input parameters to calculate the equivalent V_p and V_s for a melt fraction of 10%. Assuming a one-layer crust with equivalent V_p and V_s, we then generate synthetic RF waveforms for a crustal thickness of 35 km (Figure S10 in Supporting Information S1). The presumed parameters (Table S1 in Supporting Information S1) are perturbed when applying the H-Φ stacking to the synthetic RF waveforms. Figure S11 in Supporting Information S1 shows the derived H, V_p, V_s, V_p/V_s and Φ, which are recovered with acceptable deviations, suggesting that H-Φ stacking has weak sensitivity to the presumed parameters. Regarding the N1 model (Table S1 in Supporting Information S1), the explicit approach (e.g., H-κ stacking) produces similar melt fraction estimates to that from H-Φ stacking (with a difference of ∼1%–2%) despite using an inaccurate crustal V_p of 6.1–6.5 km/s (the true V_p is 5.7 km/s), indicating that melt fraction (i.e., V_p/V_s) is insensitive to the assumed crustal V_p value. In this case, however, the crustal thickness is notably different, with deviations as high as ∼5 km, suggesting its stronger sensitivity to the crustal V_p or melt

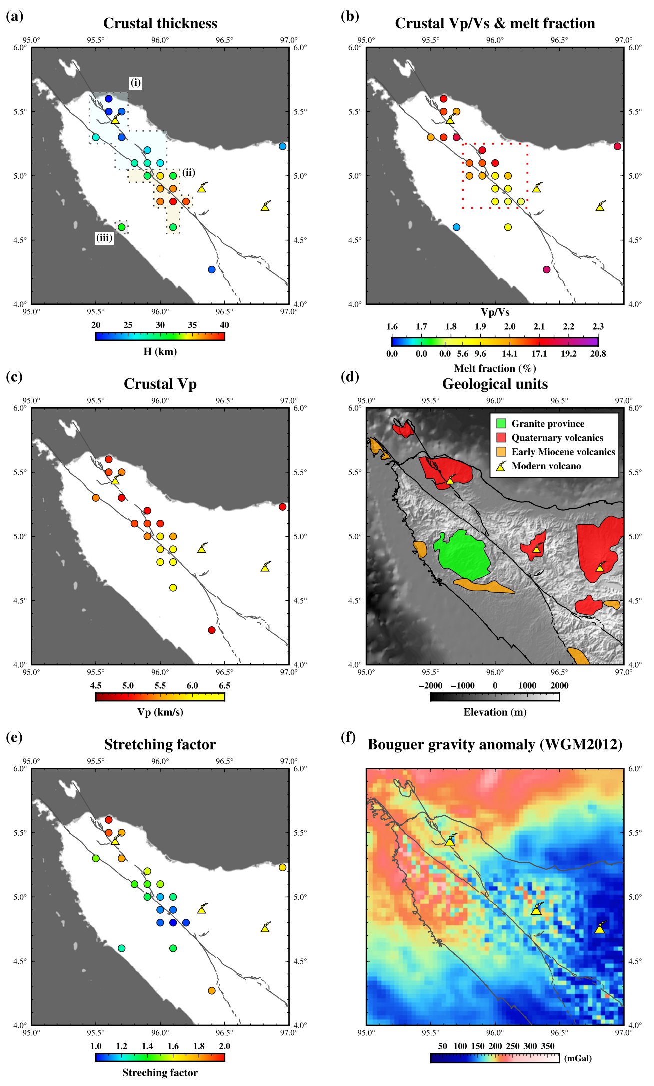

Figure 3. Spatial variations of (a) crustal thickness, (b) V_p/V_s and melt fraction, (c) V_p, (d) key geological units, (e)stretching factor, and (f) Bouguer gravity anomaly. The polygons in (a) show our sub-regions. The red rectangle in (b) highlights the area where crustal thickness and V_p/V_s show a strong negative correlation (Figure 4c).

fraction. Because H-Φ stacking overperforms the explicit approach based on H-κ stacking, in this study results are mostly derived from H-Φ stacking. We then test the influence of a uniformly dipping Moho, crustal anisotropy, and multiple crustal layers on H-Φ stacking estimates. As shown in Figures S12 and S13 in Supporting Information S1, a Moho dips at an angle <15°, or a <10% anisotropic crust with a horizontal symmetric axis, results in <~5 km and <~5% deviations in crustal thickness and melt fraction, respectively. We also find that virtual station stacking can alleviate the influence of a dipping Moho. See more details in Text S3 of Supporting Information S1.

4. Results

Reliable estimates on crustal thickness and V_p/V_s ratio by H-Φ stacking are obtained at 21 virtual stations and 2 broadband stations (Table S2 in Supporting Information S1). The crustal thickness ranges from 20 to 40 km (±1.0–6.6 km; ±3.0 km on average). The average crustal thickness is ~29 km (Figure 3a), close to the average crustal thickness in Crust1.0 for the same region (~31 km; Figure S14 in Supporting Information S1). However, our results show much stronger spatial variations. The estimated V_p/V_s ratio varies from 1.65 to 2.19 (±0.04–0.11; ±0.09 on average), with an average of ~1.98 (Figure 3b). The average V_p/V_s ratio is much higher than the global continental average of ~1.77 (Christensen, 1996), but instead is closer to the V_p/V_s ratios in active volcanic regions (1.87 and above) (Ji et al., 2009), with values higher than 1.95 reported in many volcanic areas (e.g., Janiszewski et al., 2013; Lin et al., 2020; Rao et al., 2015), including the Sunda arc (Syuhada et al., 2016; Wölbern & Rümpker, 2016). The crustal average V_p values are 4.9–6.3 km/s (±0.1–0.5 km/s; ±0.3 km/s on average), with an average of ~5.4 km/s (Figure 3c), close to the value of ~5.1 km/s in the Red Sea Rift volcanic zone (Reed et al., 2014) but much smaller than the global continental average of 6.45 km/s (Christensen & Mooney, 1995). Melt fractions are estimated to be ~0%–19% (±1.0–6.7%; ±3.7% on average), with an average of ~12% (Figures 3b and 4b), similar to the average crustal melt fraction of ~9% estimated by Reed et al. (2014). The explicit and implicit approaches provide similar melt fraction estimates, with the difference of <1% on average (Figures 2c, 2d, and 4b). Note that crustal thickness estimated from H-Φ stacking is ~0–6 km smaller than that estimated using traditional H-κ stacking (Figure S15 in Supporting Information S1), which is caused by overestimation of H-κ stacking, as we highlighted in Section 3.2 and also emphasized by Reed et al. (2014). H-Φ stacking results in a generally larger uncertainty than H-κ stacking (e.g., Figures 2c and 2d), owing to the intrinsic lower sharpness of the stacked energy contours around the peak.

We find distinguishing features of crustal structure along the GSF. At the northwestern part (i.e., region i in Figure 3a), the crust is thinner (~24 km), with higher V_p/V_s (~2.07), hence higher melt fraction (~16%), and lower average crustal V_p (~5.2 km/s). At the southeastern part, between the two GSF bifurcations (i.e., region ii), the crust is thicker (~35 km), has lower V_p/V_s (~1.88), lower melt fraction (~8%), and higher V_p (~5.9 km/s). In region ii, the uncertainty of the estimates is also larger than that in region i, suggesting higher noise contamination level and/or more complex crustal structures (Table S2 in Supporting Information S1). At the forearc area (region iii), the V_p/V_s is strikingly low (~1.65; Figure 3b).

5. Interpretation and Discussion

5.1. Pervasive Crustal Melts in Aceh and Its Global Implications

The wide range of melt fractions (0%–19%) in Aceh suggests a high spatial variation of magma distribution in the crust. The melt fraction is different in the forearc (region iii in Figure 3a) and arc-backarc areas (regions i and ii).

10.1029/2023GL104391

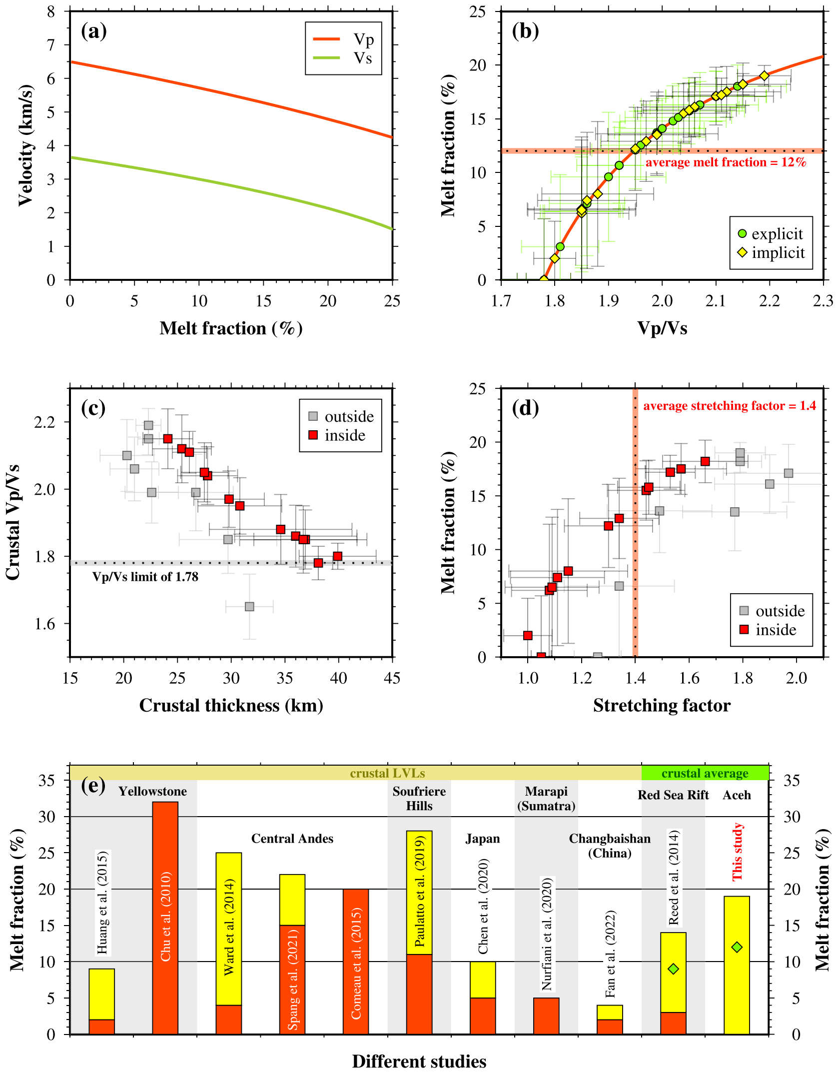

Figure 4. (a) Theoretical relationships between velocity and melt fraction, (b) melt fractions estimated by the explicit and implicit methods, (c and d) correlations between crustal thickness and V_p/V_s (i.e., stretching factor and melt fraction). The red curve in (b) shows the theoretical relationship calculated by the explicit approach. Red and gray squares in (c and d) show the crustal thickness and V_p/V_s inside and outside the Great Sumatran Fault transition (the red rectangle in Figure 3b), respectively. Panel (e) shows comparison of melt fraction with other studies. Yellow bars show the range of melt fraction with the red bars show the minimum. Red bars also show melt fractions from studies only providing an average. Green diamonds mark the regional averages.

In the arc-backarc areas, the melt fraction is ∼16% around the Seulawah Agam Volcano (region i), and gradually decreases to ∼8% further to the southeast (region ii). In the forearc area (region iii) where an intruded Cretaceous granite batholith outcropped (Barber, 2000), the crustal V_p/V_s is as low as 1.65 (i.e., 0% melt fraction), suggesting a dominantly felsic crust that has not been reignited by modern volcanism (Lai et al., 2021).

The 12% average crustal melt fraction suggests pervasive magmatic mush and partial melting in the Aceh crust. Similarly high V_p/V_s ratios and high melt fractions have been reported in other volcanic areas (e.g., Eagar et al., 2011; Janiszewski et al., 2013; Reed et al., 2014), suggesting that high melt fraction is a common feature in active volcanic regions. The melt fraction we derive represents a crustal average, which may imply the existence of localized crustal magmatic bodies with melt fractions larger than 19%. Melt fractions estimated for localized crustal Low Velocity Layers (LVLs) in a few volcanic areas indeed show large values (e.g., 20% to 30%) such as Yellowstone (Chu et al., 2010), Soufrière Hills (Paulatto et al., 2019), and Central Andes (Comeau et al., 2015; Spang et al., 2021) (Figure 4e).

In addition, relatively low melt fractions are reported for some volcanic regions, with estimates from 2% to 10% for the intra-crustal LVLs with several-kilometer thicknesses, for example, in Northeast Japan (K. X. Chen et al., 2020), Changbaishan volcano (Fan et al., 2022), and Marapi volcano (Nurfiani et al., 2021) (Figure 4e). Even for the same volcano, different studies show dramatic differences in melt fraction estimates. For example, Huang et al. (2015) reported a ~10,000 km^3 low-velocity reservoir with ~9% melt fraction beneath Yellowstone volcano using P-wave tomography. However, RF modeling presented by Chu et al. (2010) shows a ~4,300 km^3 LVL in the same area with a melt fraction of ~32%. Relatively low melt fraction estimates can be caused by the resolution limits, the wavefront healing effect, and non-uniqueness of seismic tomography techniques (Fan et al., 2022; Paulatto et al., 2019, 2022; Rasht-Behesht et al., 2020). For instance, the wavefront healing effect can lead to ~50% melt fraction underestimation (Paulatto et al., 2019). The H-Φ stacking method is more sensitive to the crustal thickness and the crustal average V_p/V_s than tomography, providing independent and complementary melt fraction constraints.

5.2. Crustal Volcanism Migration Facilitated by Crustal Stretching

The crustal thickness of ~22 km in northern Aceh is much thinner than the global average of 30.5 km for extended crust (Christensen & Mooney, 1995), suggesting much strong extensional deformation of the crust. The off-Sumatran fault seismicity in Aceh also indicates strong distributed crustal deformation (Muzli et al., 2018). To quantify the degree of crustal extension, we calculated the stretching factor assuming that the prior-stretching crustal thickness is the largest crustal thickness in the study region (39.9 km; Table S2 in Supporting Information S1) (L. Chen, 2014). The estimated stretching factors range from ~1.0–2.0 with an average of ~1.4, similar to that in other continental margins (Ahmed et al., 2013; L. Chen, 2014; L. Chen et al., 2013). The stretching factor decreases from northwest to southeast, along the spreading direction of the Andaman Sea (Figures 1a and 3e), probably suggesting a causal relationship. The spreading of the Andaman Sea has enhanced the regional geotherm to the north of the GSF, therefore facilitating the northward migration of volcanism around Seulawah Agam volcano (Lai et al., 2021). It is notable that the western branch of the bifurcation marks a boundary between two blocks of different Bouguer gravity anomaly, with a smaller positive gravity anomaly beneath Seulawah Agam volcano (Figure 3f). This sharp drop in gravity maybe due to pervasive low-density magma in the eastern crust, which has fed into the Quaternary volcanics and is shown as high melt fractions in our results. Frequent seismicity in the crust may have created faults that facilitate melt intrusion and accumulation, therefore speeding up crustal magmatism. At the branching transition of the GSF, we notice a clear negative correlation between crustal thickness and V_p/V_s, thus a positive correlation between stretching factor and melt fraction (Figures 4c and 4d), suggesting that the elevated crustal melting percentage is closely related to the fault branching.

In contrast to the Seulawah Agam volcanic area, the crustal thickness (~35 km) near the Quaternary volcanics at Peuet Sague volcano is closer to the global average (Figure 3). The Bouguer gravity anomaly at the Peuet Sague volcano is more scattered, with a larger magnitude of the anomaly than its nearby region, while gravity near the Geureudong volcanics shows no dramatic differences with its neighbors. These features suggest that the northward migration of Peuet Sague and Geureudong volcanisms may not be simply explained by crustal stretching and further investigations are needed.

5.3. Limitations and Future Study

While H-Φ stacking of RFs provides a robust estimation of the crustal melt fraction, there are several limitations. First, since the entire crust is considered as one layer, this method cannot reveal detailed crustal magmatic architecture. Second, H-Φ stacking requires more parameters than H-κ stacking, therefore suffering from more trade-offs between parameters. Third, H-Φ stacking assumes a homogeneous isotropic crust, providing estimates with <~5 km and <~5% biases in crustal thickness and melt fraction, respectively, when the Moho dip angle is <~15° and the crustal anisotropy strength is <~10%. Highly complicated crustal structures (e.g., larger crustal anisotropy, steeply dipping Moho, 3-D structure, and their compound effects) can significantly influence the melt fraction estimates. Adopting more advanced H-κ stacking techniques into H-Φ stacking will further improve the accuracy (e.g., Li et al., 2019). Finally, we exclude the contribution of volatiles in Gassmann's equations for simplification, which would act to decrease the melt fraction estimates (Chu et al., 2010). Future studies can consider volatiles to have better melt fraction estimates.

6. Conclusion

We propose a new RF method, H-Φ stacking, to constrain crustal thickness, V_p, V_p/V_s, and melt fraction simultaneously. Application to northern Sumatra dense array observations reveals a thin crust near the continental margin associated with significantly high V_p/V_s (~1.98) and melt fraction (12%), indicating pervasive magmatic mush in the crust. Our results provide new insights to the northward migration of the Seulawah Agam volcanism and its correlation with crustal seismicity.

Data Availability Statement

The seismic data used are archived at Feng and Wei (2023). Data of active volcanoes are from Global Volcanism Program (2023). Bouguer gravity anomaly data are from Bonvalot et al. (2012). We sincerely thank the Indonesian Agency for Meteorology, Climatology, and Geophysics for providing the permanent seismic station data, LHMI and MLSI (IA network), which are downloaded from 202.90.198.100/webdc3/ when it was accessible. The data are also achieved at the GEOFON center with restricted access currently. We use hk1.3 software package (Zhu, 2009) to calculate RFs and do H-κ stacking.We use RAYSUM software (Frederiksen & Bostock, 2000) to calculate synthetic seismic waveforms in the cases of anisotropic layers and dipping interfaces. H-Φ stacking and virtual station stacking codes are available at Feng et al. (2023).

Acknowledgments

We thank editor Christian Huber, reviewer Ayush Goyal, and another anonymous reviewer for their helpful comments. This research is jointly supported by the National Natural Science Foundation of China (42288201) and the Ministry of Education, Singapore, under its MOE Academic Research Fund Tier 3 (Award MOE-MOET32021-0002). This work comprises EOS contribution number 546.

References

Ahmed, A., Tiberi, C., Leroy, S., Stuart, G. W., Keir, D., Sholan, J., et al. (2013). Crustal structure of the rifted volcanic margins and uplifted plateau of western Yemen from receiver function analysis. *Geophysical Journal International*, *193*(3), 1673–1690. https://doi.org/10.1093/gji/ggt072

Annen, C., Blundy, J. D., & Sparks, R. S. J. (2006). The genesis of intermediate and silicic magmas in deep crustal hot zones. *Journal of Petrology*, *47*(3), 505–539. https://doi.org/10.1093/petrology/egi084

Barber, A. J. (2000). The origin of the Woyla Terranes in Sumatra and the Late Mesozoic evolution of the Sundaland margin. *Journal of Asian Earth Sciences*, *18*(6), 713–738. https://doi.org/10.1016/S1367-9120(00)00024-9

Bass (1995). Elasticity of minerals, glasses, and melts. In *Mineral physics and crystallography: A handbook of physical constants* (pp. 45–63).

Bonvalot, S., Briais, A., Kuhn, M., Peyrefitte, A., Vales, N., Biancale, R., et al. (2012). World Gravity Map WGM2012 [Dataset]. Bureau Gravimétrique International. https://doi.org/10.18168/bgi.23

Bora, D. K., Borah, K., & Goyal, A. (2016). Crustal shear-wave velocity structure beneath Sumatra from receiver function modeling. *Journal of Asian Earth Sciences*, *121*, 127–138. https://doi.org/10.1016/j.jseaes.2016.03.007

Cashman, K. V., Sparks, R. S. J., & Blundy, J. D. (2017). Vertically extensive and unstable magmatic systems: A unified view of igneous processes. *Science*, *355*(6331), eaag3055. https://doi.org/10.1126/science.aag3055

Chen, K. X., Fischer, K. M., Hua, J., & Gung, Y. (2020). Imaging crustal melt beneath northeast Japan with Ps receiver functions. *Earth and Planetary Science Letters*, *537*, 116173. https://doi.org/10.1016/j.epsl.2020.116173

Chen, L. (2014). Stretching factor estimation for the long-duration and multi-stage continental extensional tectonics: Application to the Baiyun Sag in the northern margin of the South China Sea. *Tectonophysics*, *611*, 167–180. https://doi.org/10.1016/j.tecto.2013.11.026

Chen, L., Zhang, Z., & Song, H. (2013). Weak depth and along-strike variations in stretching from a multi-episodic finite stretching model: Evidence for uniform pure-shear extension in the opening of the South China Sea. *Journal of Asian Earth Sciences*, *78*, 358–370. https://doi.org/10.1016/j.jseaes.2012.12.033

Chlieh, M., Avouac, J. P., Hjorleifsdottir, V., Song, T. R. A., Ji, C., Sieh, K., et al. (2007). Coseismic slip and afterslip of the great Mw 9.15 Sumatra-Andaman earthquake of 2004. *Bulletin of the Seismological Society of America*, *97*(1A), S152–S173. https://doi.org/10.1785/0120050631

Christensen, N. I. (1996). Poisson's ratio and crustal seismology. *Journal of Geophysical Research*, *101*(B2), 3139–3156. https://doi.org/10.1029/95jb03446

Christensen, N. I., & Mooney, W. D. (1995). Seismic velocity structure and composition of the continental crust: A global view. *Journal of Geophysical Research*, *100*(B6), 9761–9788. https://doi.org/10.1111/j.1755-6724.2004.tb00702.x

Chu, R., Helmberger, D. V., Sun, D., Jackson, J. M., & Zhu, L. (2010). Mushy magma beneath Yellowstone. *Geophysical Research Letters*, *37*(1), L01306. https://doi.org/10.1029/2009GL041656

Collings, R., Lange, D., Rietbrock, A., Tilmann, F., Natawidjaja, D., Suwargadi, B., et al. (2012). Structure and seismogenic properties of the Mentawai segment of the Sumatra subduction zone revealed by local earthquake traveltime tomography. *Journal of Geophysical Research*, *117*(B1), B01312. https://doi.org/10.1029/2011JB008469

Comeau, M. J., Unsworth, M. J., Ticona, F., & Sunagua, M. (2015). Magnetotelluric images of magma distribution beneath Volcán Uturuncu, Bolivia: Implications for magma dynamics. *Geology*, *43*(3), 243–246. https://doi.org/10.1130/G36258.1

Eagar, K. C., Fouch, M. J., James, D. E., & Carlson, R. W. (2011). Crustal structure beneath the High Lava Plains of eastern Oregon and surrounding regions from receiver function analysis. *Journal of Geophysical Research*, *116*(2), B02313. https://doi.org/10.1029/2010JB007795

Fan, X., Guo, Z., Zhao, Y., & Chen, Q. F. (2022). Crust and uppermost mantle magma plumbing system beneath changbaishan intraplate volcano, China/North Korea, revealed by ambient noise adjoint tomography. *Geophysical Research Letters*, *49*(12), e2022GL098308. https://doi.org/10.1029/2022GL098308

Feng, M., Chen, L., Wang, X., Wei, S., & Wang, X. (2021). Crustal structure and its tectonic implications in Sundaland and adjacent areas: Constraints from tele-seismic receiver functions. *Chinese Journal of Geophysics*, *64*(12), 4364–4377. (in Chinese). https://doi.org/10.6038/cjg2021O0356

Feng, M., & Wei, S. (2023). Seismic receiver function data of Aceh, Indonesia (Version 2.0) [Dataset]. DR-NTU. https://doi.org/10.21979/N9/KVO4JM

Feng, M., Wei, S., & Chen, L. (2023). Seismic receiver function H-Phi stacking to estimate crustal thickness and melt fraction [Software]. Zenodo. https://doi.org/10.5281/zenodo.10040890

Frederiksen, A. W., & Bostock, M. G. (2000). Modelling teleseismic waves in dipping anisotropic structures. *Geophysical Journal International*, *141*(2), 401–412. https://doi.org/10.1046/j.1365-246x.2000.00090.x

Gassmann (1951). Uber die elastizitat poroser medien. *Verteljahrss- Chrift Der Naturforschenden Gesellschaft in Zurich*, *96*, 1–23.

Global Volcanism Program. (2023). Volcanoes of the world (v. 5.1.1) [Database]. *Distributed by Smithsonian Institution, compiled by Venzke, E.* https://doi.org/10.5479/si.GVP.VOTW5-2023.5.1

Hammond, J. O. S. (2014). Constraining melt geometries beneath the Afar Depression, Ethiopia from teleseismic receiver functions: The anisotropic H-κ stacking technique. *Geochemistry, Geophysics, Geosystems*, *15*(14), 1316–1332. https://doi.org/10.1002/2013GC005186.Received

Hsu, Y. J., Simons, M., Avouac, J. P., Galetzka, J., Sieh, K., Chlieh, M., et al. (2006). Frictional afterslip following the 2005 Nias-Simeulue earthquake, Sumatra. *Science*, *312*(5782), 1921–1926. https://doi.org/10.1126/science.1126960

Huang, H. H., Lin, F. C., Schmandt, B., Farrell, J., Smith, R. B., & Tsai, V. C. (2015). The Yellowstone magmatic system from the mantle plume to the upper crust. *Science*, *348*(6236), 773–776. https://doi.org/10.1126/science.aaa5648

Janiszewski, H. A., Abers, G. A., Shillington, D. J., & Calkins, J. A. (2013). Crustal structure along the Aleutian island arc: New insights from receiver functions constrained by active-source data. *Geochemistry, Geophysics, Geosystems*, *14*(8), 2977–2992. https://doi.org/10.1002/ggge.20211

Ji, S., Wang, Q., & Salisbury, M. H. (2009). Composition and tectonic evolution of the Chinese continental crust constrained by Poisson's ratio. *Tectonophysics*, *463*(1–4), 15–30. https://doi.org/10.1016/j.tecto.2008.09.007

Kennett, B. L. N., Engdahl, E. R., & Buland, R. (1995). Constraints on seismic velocities in the Earth from traveltimes. *Geophysical Journal International*, *122*(1), 108–124. https://doi.org/10.1111/j.1365-246X.1995.tb03540.x

Kikuchi, M., & Kanamori, H. (1992). Inversion of complex body waves. *Bulletin of the Seismological Society of America*, *72*(2), 491–506.

Lai, Y. M., Chung, S. L., Ghani, A. A., Murtadha, S., Lee, H. Y., & Chu, M. F. (2021). Mid-Miocene volcanic migration in the westernmost Sunda arc induced by India-Eurasia collision. *Geology*, *49*(6), 713–717. https://doi.org/10.1130/G48568.1

Langston, C. A. (2011). Wave-field continuation and decomposition for passive seismic imaging under deep unconsolidated sediments. *Bulletin of the Seismological Society of America*, *101*(5), 2176–2190. https://doi.org/10.1785/0120100299

Laske, G., Masters, G., Ma, Z., & Pasyanos, M. E. (2012). CRUST1.0: An updated global model of Earth's crust. *Geophysical Research Abstracts EGU General Assembly*, *14*, 2012–3743.

Li, J., Song, X., Wang, P., & Zhu, L. (2019). A generalized H-κ method with harmonic corrections on Ps and its crustal multiples in receiver functions. *Journal of Geophysical Research: Solid Earth*, *124*(4), 3782–3801. https://doi.org/10.1029/2018JB016356

Ligorría, J. P., & Ammon, C. J. (1999). Iterative deconvolution and receiver-function estimation. *Bulletin of the Seismological Society of America*, *89*(5), 1395–1400. https://doi.org/10.1785/bssa0890051395

Lin, C. M., Tseng, T. L., Meliksetian, K., Karakhanyan, A., Huang, B. S., Babayan, H., et al. (2020). Locally thin crust and high crustal V_P/V_S ratio beneath the Armenian volcanic highland of the Lesser Caucasus: A case for recent delamination. *Journal of Geophysical Research: Solid Earth*, *125*(9), e2019JB019151. https://doi.org/10.1029/2019JB019151

Lythgoe, K., Muksin, M., Simanjuntak, A., Andrean, S., & Wei, S. (2022). Striking out into the field to track Slip on the Sumatran Fault. *Eos*, *103*(7), 31–36. https://doi.org/10.1029/2022eo220140

Lythgoe, K. H., Ong Su Qing, M., & Wei, S. (2020). Large-scale crustal structure beneath Singapore using receiver functions from a dense urban nodal array. *Geophysical Research Letters*, *47*(7), e2020GL087233. https://doi.org/10.1029/2020GL087233

Macpherson, K. A., Hidayat, D., & Goh, S. H. (2012). Receiver function structure beneath four seismic stations in the Sumatra region. *Journal of Asian Earth Sciences*, *46*, 161–176. https://doi.org/10.1016/j.jseaes.2011.12.005

Muksin, U., Bauer, K., Muzli, M., Ryberg, T., Nurdin, I., Masturiyono, M., & Weber, M. (2019). AcehSeis project provides insights into the detailed seismicity distribution and relation to fault structures in Central Aceh, Northern Sumatra. *Journal of Asian Earth Sciences*, *171*, 20–27. https://doi.org/10.1016/j.jseaes.2018.11.002

Muzli, M., Muksin, U., Nugraha, A. D., Bradley, K. E., Widiyantoro, S., Erbas, K., et al. (2018). The 2016 Mw 6.5 Pidie Jaya, Aceh, North Sumatra, earthquake: Reactivation of an unidentified sinistral fault in a region of distributed deformation. *Seismological Research Letters*, *89*(5), 1761–1772. https://doi.org/10.1785/0220180068

Niu, F., & Li, J. (2011). Component azimuths of the CEArray stations estimated from P-wave particle motion. *Earthquake Science*, *24*(1), 3–13. https://doi.org/10.1007/s11589-011-0764-8

Nur, A., Gary, M., Jack, D., & Doron, G. (1998). Critical porosity: The key to relating physical properties to porosity in rocks. *The Leading Edge*, 357–362. https://doi.org/10.1190/1.1887540

Nurfiani, D., Wang, X., Gunawan, H., Triastuty, H., Hidayat, D., Wei, S. J., et al. (2021). Combining petrology and seismology to unravel the plumbing system of a typical arc volcano: An example from Marapi, West Sumatra, Indonesia. *Geochemistry, Geophysics, Geosystems*, *22*(4), e2020GC009524. https://doi.org/10.1029/2020GC009524

Ogden, C. S., Bastow, I. D., Gilligan, A., & Rondenay, S. (2019). A reappraisal of the H–κ stacking technique: Implications for global crustal structure. *Geophysical Journal International*, *219*(3), 1491–1513. https://doi.org/10.1093/gji/ggz364

Paulatto, M., Hooft, E. E. E., Chrapkiewicz, K., Heath, B., Toomey, D. R., & Morgan, J. V. (2022). Advances in seismic imaging of magma and crystal mush. *Frontiers in Earth Science*, *10*, 970131. https://doi.org/10.3389/feart.2022.970131

Paulatto, M., Moorkamp, M., Hautmann, S., Hooft, E., Morgan, J. V., & Sparks, R. S. J. (2019). Vertically extensive magma reservoir revealed from joint inversion and quantitative interpretation of seismic and gravity data. *Journal of Geophysical Research: Solid Earth*, *124*(11), 11170–11191. https://doi.org/10.1029/2019JB018476

Pratama, R., Ariyanto, P., Wijaya, A., & Ariwibowo, S. (2020). Identification of Moho discontinuity depth variations and subduction slab in north Sumatra region using receiver function method. *Journal of Physics: Conference Series*, *1491*(1), 012052. https://doi.org/10.1088/1742-6596/1491/1/012052

Rao, K. M., Kumar, M. R., & Rastogi, B. K. (2015). Crust beneath the northwestern Deccan volcanic province, India: Evidence for uplift and magmatic underplating. *Journal of Geophysical Research: Solid Earth*, *120*(5), 3385–3405. https://doi.org/10.1002/2014JB011819

Rasht-Behesht, M., Huber, C., & Mancinelli, N. J. (2020). Detectability of melt-rich lenses in magmatic reservoirs from teleseismic waveform modeling. *Journal of Geophysical Research: Solid Earth*, *125*(9). https://doi.org/10.1029/2020JB020264

Reed, C. A., Almadani, S., Gao, S. S., Elsheikh, A. A., Cherie, S., Abdelsalam, M. G., et al. (2014). Receiver function constraints on crustal seismic velocities and partial melting beneath the Red Sea rift and adjacent regions, Afar Depression. *Journal of Geophysical Research: Solid Earth*, *119*(3), 2138–2152. https://doi.org/10.1002/2013JB010719

Rock, N. M. S., Syah, H. H., Davis, A. E., Hutchison, D., Styles, M. T., & Lena, R. (1982). Permian to recent volcanism in northern Sumatra, Indonesia: A preliminary study of its distribution, chemistry, and peculiarities. *Bulletin Volcanologique*, *45*(2), 127–152. https://doi.org/10.1007/BF02600429

Spang, A., Baumann, T. S., & Kaus, B. J. P. (2021). A multiphysics approach to constrain the dynamics of the Altiplano-Puna magmatic system. *Journal of Geophysical Research: Solid Earth*, *126*(7), e2021JB021725. https://doi.org/10.1029/2021JB021725

Syuhada, S., Hananto, N. D., Abdullah, C. I., Puspito, N. T., Anggono, T., & Yudistira, T. (2016). Crustal structure along Sunda-Banda arc transition zone from teleseismic receiver functions. *Acta Geophysica*, *64*(6), 2020–2050. https://doi.org/10.1515/acgeo-2015-0098

Van der Molen, I., & Paterson, M. S. (1979). Experimental deformation of partially-melted granite. *Contributions to Mineralogy and Petrology*, *70*(3), 299–318. https://doi.org/10.1007/bf00375359

Wang, T., Gao, S. S., Yang, Q., & Liu, K. H. (2021). Crustal structure beneath the Ethiopian Plateau and adjacent areas from receiver functions: Implications for partial melting and magmatic underplating. *Tectonophysics*, *809*, 228857. https://doi.org/10.1016/j.tecto.2021.228857

Wang, X., Chen, Q., Li, J., & Wei, S. (2016). Seismic sensor misorientation measurement using P-wave particle motion: An application to the NECsaids array. *Seismological Research Letters*, *87*(4), 901–911. https://doi.org/10.1785/0220160005

Wang, X., Liu, X., Zhao, D., Liu, B., Qiao, Q., Zhao, L., & Wang, X. (2022). Oceanic plate subduction and continental extrusion in Sumatra: Insight from S-wave anisotropic tomography. *Earth and Planetary Science Letters*, *580*, 117388. https://doi.org/10.1016/j.epsl.2022.117388

Ward, K. M., Lin, F., & Schmandt, B. (2018). High-resolution receiver function imaging across the Cascadia subduction zone using a dense nodal array. *Geophysical Research Letters*, *45*(22), 12218–12225. https://doi.org/10.1029/2018GL079903

Watanabe, T. (1993). Effects of water and melt on seismic velocities and their application to characterization of seismic reflectors. *Geophysical Research Letters*, *20*(24), 2933–2936. https://doi.org/10.1029/93GL03170

Wölbern, I., & Rümpker, G. (2016). Crustal thickness beneath Central and East Java (Indonesia) inferred from P receiver functions. *Journal of Asian Earth Sciences*, *115*, 69–79. https://doi.org/10.1016/j.jseaes.2015.09.001

Yu, X., & Lee, C. T. A. (2016). Critical porosity of melt segregation during crustal melting: Constraints from zonation of peritectic garnets in a dacite volcano. *Earth and Planetary Science Letters*, *449*, 127–134. https://doi.org/10.1016/j.epsl.2016.05.025

Yu, Y., Song, J., Liu, K. H., & Gao, S. S. (2015). Determining crustal structure beneath seismic stations overlying a low-velocity sedimentary layer using receiver functions. *Journal of Geophysical Research: Solid Earth*, *120*(5), 3208–3218. https://doi.org/10.1002/2014JB011610

Zaini, N., Yanis, M., Marwan, A., Isa, M., & van der Meer, F. (2021). Assessing of land surface temperature at the Seulawah Agam volcano area using the Landsat series imagery. *Journal of Physics: Conference Series*, *1825*(1), 012021. https://doi.org/10.1088/1742-6596/1825/1/012021

Zelt, B. C., & Ellis, R. M. (1999). Receiver-function studies in the Trans-Hudson Orogen, Saskatchewan. *Canadian Journal of Earth Sciences*, *36*(4), 585–603. https://doi.org/10.1139/e98-109

Zhu, L. (2009). Receiver function package (deconvolution and H-κ stacking) hk1.3 (Version 1.3) [Software]. Saint Louis University. Retrieved from https://www.eas.slu.edu/People/LZhu/home.html

Zhu, L., & Kanamori, H. (2000). Moho depth variation in southern California from teleseismic receiver functions. *Journal of Geophysical Research*, *105*(B2), 2969–2980. https://doi.org/10.1029/1999JB900322